Check for updates

Shear-driving Force and Critical Shear Angle Analysis of Kevlar/Carbon Fiber Hybrid Composite Skins for a Shear Variable-sweep Wing Based on the Classical Plate Theory

Guang Yang[1] · Hongwei Guo[1] · Hong Xiao[1] · Rongqiang Liu[1] · Chuang Shi[1]

Abstract

The morphing skin that can be used for the shear variable-sweep wing is of great significance to improve the aerodynamic efficiency of the aircraft. In this paper, the Kevlar/carbon fiber hybrid composite skins that can be smoothly and continuously sheared are applied. Moreover, the shear driving force and critical shear angle of the hybrid composite skins are studied. Based on the classical plate theory, the nonlinear mathematical model is developed for the shear-driving force and critical shear angle of composite skins. Based on the principle of virtual work and the fundamental lemma of calculus of variations, the motion equations are derived and the closed-form solutions are obtained for sutured composite skins on the framework. A systematic comparison between the theoretical solutions and experimental results is carried out to validate the excellent accuracy and reliability of the numerical evaluations. The effects of geometric and material parameters on the shear-driving force and critical shear angle of composite skins are systematically studied. The results show that the carbon fiber diameter, carbon fiber spacing, together with the length and width of skin cell have a significant impact on the shear-driving force and critical shear angle of composite skins.

1 Introduction

According as the demand for multi-functional and high-efficiency aircraft in aerospace field increases, the morphing wing has rapidly become a hot spot in aerospace technology innovation field [1, 2]. Compared with the fixed wing, the morphing wing can flexibly change its shape with the change of environment, task, enhance flight performance

---

✉ Hongwei Guo
guohw@hit.edu.cn

✉ Hong Xiao
xiaohong@hit.edu.cn

1   State Key Laboratory of Robotics and System, Harbin Institute of Technology, Harbin 150001, China

and efficiency [1, 2]. The most representative of the morphing wings is the variable-sweep wing. The variable-sweep wing can change the sweep angle according to the flight speed to improve the aerodynamic efficiency of the aircraft. In recent years, the shear variable-sweep wing has been proposed, which has better deformation scale and aerodynamic performance [3, 4]. However, the development of shear variable-sweep wing has arose the demand for morphing skin that need to ensure smooth aerodynamic surface and low in-plane stiffness during shear deformation [5]. Therefore, it is significant to propose a new type of morphing skin for the shear variable-sweep wing and study its driving force and smooth characteristics.

In the past two decades, researchers have developed and examined a variety of skins based on shear deformation requirements. Grant et al. [6] introduced a morphing skin with a multiple-joint design that allows variations in sweep. However, the surface of this skin is not smooth and the sealing is relatively poor. Keihl et al. [7] studied the characteristics of shape memory polymer as a shear morphing skin. Although the multi-state ability of shape memory polymer makes it easy to change shape, the surface is not smooth. Olympio et al. [8] designed a flexible skin comprising of a cellular substructure and pre-tensioned facesheet for a shear morphing wing. Laila et al. [9] optimized and tested the pre-tensioned skin in wind tunnel and flight tests. The pre-strain can alleviate facesheet wrinkling, but it will lead to the creep of the elastic material and short service life. In these studies, many skins for the shear variable-sweep wings were designed and invented. However, these skins cannot meet the needs of high out-of-plane rigidity, low in-plane rigidity, smooth shear deformation and long service life. This work applies the Kevlar/carbon fiber hybrid composite skins to a shear variable-sweep wing. In order to understand the mechanical properties of Kevlar/carbon fiber hybrid composite skins, especially the smoothness and driving ability during the deformation process, it is necessary to establish a mathematical model for the shear-driving force and buckling load of composite skins to reveal the action mechanism of composite skins under complex flight conditions, and lay the foundation for the design and evaluation of shear variable-sweep wing.

In the analysis of the mechanical behavior of the hybrid composite skin, the hybrid composite skin is usually equivalent to a uniformly continuous orthotropic plate. Recently, many experts have proposed different higher-order shear deformation theories [10–15] to analyze the deformation of composite plates. Based on these shear deformation theories, researchers carry out a lot of theoretical studies on the bending and buckling of composite materials. Sabri and Meguid [16] investigated the wrinkling behavior of laminated orthotropic composite panels due to in-plane shear deformation. Static analysis was carried out to establish the shear-induced stress distribution patterns in the elastic panels assuming no wrinkling. Ni et al. [17] presented a buckling analysis for a rectangular laminated composite plate subjected to biaxial compression loading. The higher-order shear deformation theory was employed and a special displacement function was introduced into the Rayleigh–Ritz method. Dash and Singh [18] addressed the buckling and post-buckling of laminated composite plates using higher order shear deformation theory associated with Green–Lagrange non-linear strain–displacement relationships. Thai and Vo [19] developed a new sinusoidal four-unknown shear deformation theory for bending, buckling, and vibration of functionally graded plates. Thakur et al. [20] examined geometrically nonlinear dynamic analysis of laminated composite plate using a nonpolynomial shear deformation theory. The present formulation utilizes both von Kármán and Green–Lagrange type of strain–displacement relations to model the geometric nonlinearity. In order to analyze the differences of these higher-order shear theories, Aydogdu [21] compared four shear deformation theories for analyzing the buckling behaviors of rectangular symmetric cross-ply

plates. The study revealed that the parabolic shear deformation theory gives the buckling loads more accurate. It is worth noting that these traditional composite material studies did not consider the nonlinearity of the shear theory. In order to improve the accuracy of the analysis, the nonlinearity of the shear theory can be considered in the analysis model.

In this paper, the Kevlar/carbon fiber hybrid composite skins for a shear variable sweep wing is proposed and applied, and the shear driving force and critical shear angle of the hybrid composite skins are studied. The hybrid composite skins are taken as an orthotropic multi-layered plate. The classical plate theory (CPT) is employed. Based on the principle of virtual work and the fundamental lemma of calculus of variations, governing equations are derived and the geometrically nonlinear closed-form solutions for sutured composited skins on the framework are obtained using the Navier's technique. The validity of the theoretical solutions is demonstrated through comparison with the results from the experimental results. The effects of geometric parameters on shear-driving force and critical shear angle are systematically explored.

2 Mathematical Formulation

This paper proposed a shear variable-sweep wing which is composed of multiple identical parallelogram cells. With the increase of sweep angle, the parallelogram cells are transformed from the initial rectangular state to the parallelogram state. The Kevlar/carbon fiber hybrid composite skins are applied as shown in Fig. 1.

With reference to Fig. 2a, a purely shear-deformed parallelogram cell comprising a shear-deformable parallelogram frame and a carbon fiber/Kevlar hybrid composite skin are extracted from the shear variable-sweep wing. In order to ensure smoothness, the composite skin is stitched on the frame. The shear deformation of parallelogram cell is driven by diagonal shear-driving force. When the frame is sheared, the skin is sheared along with the frame as shown in Fig. 2b. With the gradual increase of the shear angle, the skin buckles and wrinkles. The shear angle of skin buckling is the critical shear angle.

At the micro scale, the Kevlar/carbon fiber hybrid composite skin is defined as a laminate composed of carbon fiber reinforced silicone rubber based unidirectional laminate and Kevlar reinforced silicone rubber based unidirectional laminate, as shown in Fig. 2c.
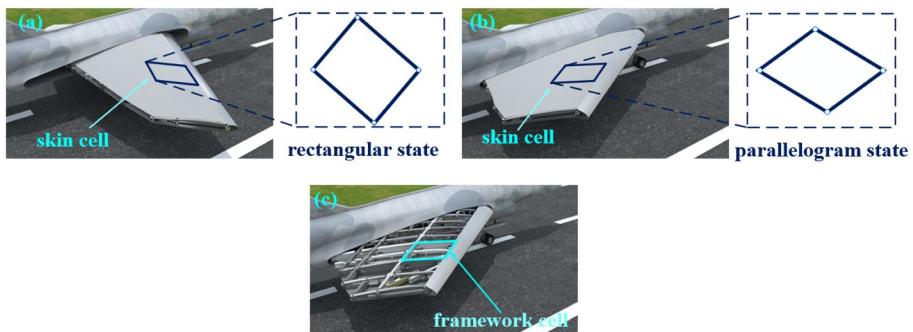

Fig. 1 The variable-swept wing based on parallelogram cell: **a** small sweep-angle state (the skin cell is rectangular); **b** large sweep-angle state (the skin cell is parallelogram); **c** the framework cell in the large sweep-angle state
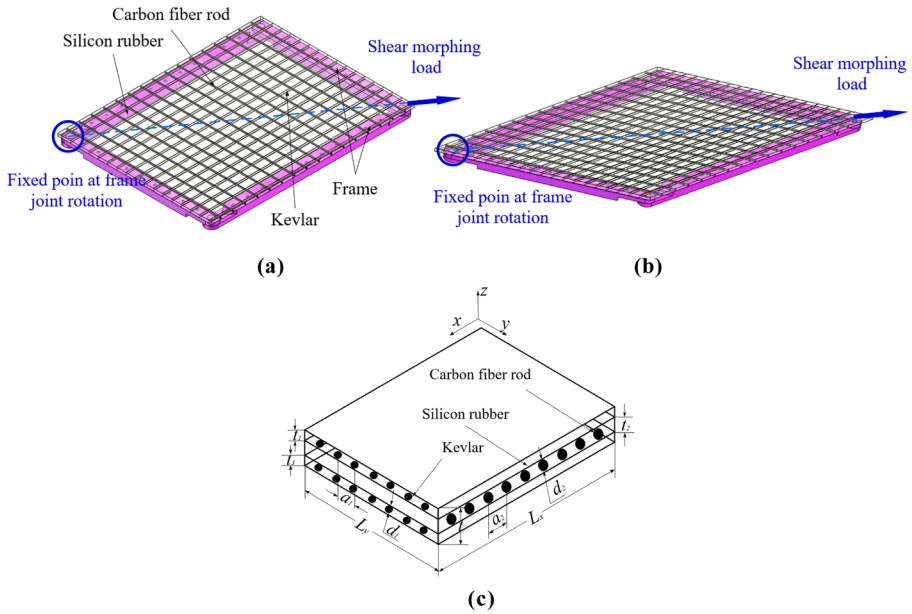
Fig. 2 A parallelogram cell composed of a frame and a Kevlar/carbon fiber composite skin: **a** the cell in the initial state (the frame is rectangular); **b** the cell in shear deformation state (frame is parallelogram); **c** the geometrical model of composite skin

Relevant geometric variables are: composite skin length L_x, width L_y, and total thickness t; Kevlar-reinforced unidirectional laminate thickness t_1; carbon fiber -reinforced unidirectional laminate thickness t_2; Kevlar diameter d_1, carbon fiber diameter d_2; Kevlar spacing a_1, carbon fiber spacing a_2.

2.1 Generalized Displacement Field and Constitutive Equation

Based on the classical plate theory (CPT) [22], the displacement field relations of composite skin take the following form:

$$u(x,y,z) = u_0 - z\frac{\partial w_b}{\partial x} - z\frac{\partial w_s}{\partial x}, \quad v(x,y,z) = v_0 - z\frac{\partial w_b}{\partial y} - z\frac{\partial w_s}{\partial y}, \quad w(x,y,z) = w_b + w_s$$

(1)

where u_0 and v_0 denote the displacements along the x-direction and y-direction of a point on the midplane of the composite skin, w_b is the bending component of the transverse displacement, w_s is the shear component of the transverse displacement, z is the shape function employed by plate theory for generalized displacement field.

Based on the von Karman strain–displacement relation [22], the strain components related to the displacement field relations of composite skin can be obtained. According to the mesomechanical analysis theory of single-layer composite materials, the material parameters of single-layer composite materials can be calculated by the material parameters of the matrix and the fiber reinforcement. Bases on the commonly mechanical analysis method of composite materials [23], the elastic modulus, shear modulus,

thermal expansion coefficients and Poisson's ratio of carbon fiber–reinforced layer and Kevlar-reinforced layer can be stated as [23]:

$$
\begin{aligned}
&E_x^{(1)} = E_x^{(3)} = E_k \frac{\pi d_1^2}{4a_1 t_1} + E_s(1 - \frac{\pi d_1^2}{4a_1 t_1})c_{fsk}, E_x^{(2)} = \frac{4a_2 t_2 E_s}{(4a_2 t_2 - \pi d_2^2) + \pi d_2^2 (E_s/E_c)} \\
&E_y^{(1)} = E_y^{(3)} = \frac{4a_1 t_1 E_s}{(4a_1 t_1 - \pi d_1^2) + \pi d_1^2 (E_s/E_k)}, E_y^{(2)} = E_c \frac{\pi d_2^2}{4a_2 t_2} + E_s(1 - \frac{\pi d_2^2}{4a_2 t_2}) \\
&v_{xy}^{(1)} = v_{xy}^{(3)} = \frac{E_y^{(1)}}{E_x^{(1)}} v_{yx}^{(1)}, v_{xy}^{(2)} = v_c \frac{\pi d_2^2}{4a_2 t_2} + v_s(1 - \frac{\pi d_2^2}{4a_2 t_2}), v_{yx}^{(1)} = v_{yx}^{(3)} = v_k \frac{\pi d_1^2}{4a_1 t_1} + v_s(1 - \frac{\pi d_1^2}{4a_1 t_1}), v_{yx}^{(2)} = \frac{E_x^{(2)}}{E_y^{(2)}} v_{xy}^{(2)} \\
&G_{xy}^{(1)} = G_{xy}^{(3)} = \frac{4a_1 t_1 G_s}{(4a_1 t_1 - \pi d_1^2) + \pi d_1^2 (G_s/G_k)}, G_{xy}^{(2)} = \frac{4a_2 t_2 G_s}{(4a_2 t_2 - \pi d_2^2) + \pi d_2^2 (G_s/G_c)}
\end{aligned}
\tag{2}
$$

where E_s, E_k, and E_c are the young's modulus of silicone rubber matrix, Kevlar and carbon fiber respectively; v_s, v_k, and v_c are the poisson's ratio of silicone rubber matrix, Kevlar and carbon fiber respectively; G_s, G_k, and G_c are the shear modulus of silicone rubber matrix, Kevlar and carbon fiber respectively. Since the fiber reinforcement directions are orthogonal to each other, the composite skin is equivalent to an orthotropic laminate. Based on the stress–strain relationship of single-layer composites [22, 23], the constitutive relations of different layers of composite skin can be obtained.

2.2 Plate Equations

According to Hamilton's principle, the control balance equation of the composite skins can be stated in an analytical form as:

$$
\delta \prod = \delta U + \delta V = 0
\tag{3}
$$

where δU is the variation of strain energy; δV is the variation of potential energy. Based on variational method, the variations of strain energy relative to the initial configuration is expressed as:

$$
\begin{aligned}
\delta U &= \sum_{k=1}^{3} \int_{t_k}^{t_{k+1}} \int_0^{L_x} \int_0^{L_y} \left(\sigma_x \delta\varepsilon_x + \sigma_y \delta\varepsilon_y + \tau_{xy}\delta\gamma_{xy} + \tau_{xz}\delta\gamma_{xz} + \tau_{yz}\delta\gamma_{yz} \right) dxdydz \\
&= \int_0^{L_x} \int_0^{L_y} \left\{ N_x \left(\frac{\partial \delta u_0}{\partial x} + \frac{\partial w}{\partial x} \frac{\partial \delta w}{\partial x} \right) - M_x^b \frac{\partial^2 \delta w_b}{\partial x^2} - M_x^s \frac{\partial^2 \delta w_s}{\partial x^2} + N_y \left(\frac{\partial \delta v_0}{\partial y} + \frac{\partial w}{\partial y} \frac{\partial \delta w}{\partial y} \right) - M_y^b \frac{\partial^2 \delta w_b}{\partial y^2} - M_y^s \frac{\partial^2 \delta w_s}{\partial y^2} \right. \\
&\left. + N_{xy} \left(\frac{\partial \delta u_0}{\partial y} + \frac{\partial \delta v_0}{\partial x} \right) + N_{xy} \left(\frac{\partial w}{\partial y} \frac{\partial \delta w}{\partial x} + \frac{\partial w}{\partial x} \frac{\partial \delta w}{\partial y} \right) - 2M_{xy}^b \frac{\partial^2 \delta w_b}{\partial x \partial y} - 2M_{xy}^s \frac{\partial^2 \delta w_s}{\partial x \partial y} + Q_{xz} \frac{\partial \delta w_s}{\partial x} + Q_{yz} \frac{\partial \delta w_s}{\partial y} \right\} dxdy
\end{aligned}
\tag{4}
$$

where N_x, N_y and N_{xy} denote the total in-plane force resultants, M_x^b, M_y^b and M_{xy}^b denote the total moment resultants, M_x^s, M_y^s and M_{xy}^s denote the additional stress couples associated with the transverse shear effects. N_x, N_y, N_{xy}, M_x^b, M_y^b, M_{xy}^b, M_x^s, M_y^s and M_{xy}^s can all be expressed by the plate stiffness coefficient, which are defined in [22].

Since the composite skins mainly bears the in-plane shear loading, the variation of work done by external forces can be expressed as:

$$
\delta V = -\int_0^{L_x} \int_0^{L_y} \left\{ N_x^s \frac{\partial w}{\partial x} \frac{\partial \delta w}{\partial x} + N_y^s \frac{\partial w}{\partial y} \frac{\partial \delta w}{\partial y} + 2N_{xy}^s \frac{\partial w}{\partial x} \frac{\partial \delta w}{\partial y} \right\} dxdy
\tag{5}
$$

Substituting the expressions for δU and δV from Eqs. (4) and (5) into Eq. (3) and integrating by parts, and collecting the coefficients of δu_0, δv_0, δw_b, and δw_s, the following equations of motion of the plate are obtained:

$$\delta u_0 : \frac{\partial N_x}{\partial x} + \frac{\partial N_{xy}}{\partial y} = 0$$

$$\delta v_0 : \frac{\partial N_{xy}}{\partial x} + \frac{\partial N_y}{\partial y} = 0$$

$$\delta w_b : \frac{\partial^2 M_x^b}{\partial x^2} + 2\frac{\partial^2 M_{xy}^b}{\partial x \partial y} + \frac{\partial^2 M_y^b}{\partial y^2} + N_x^s \frac{\partial^2 w}{\partial x^2} + N_y^s \frac{\partial^2 w}{\partial y^2} + 2N_{xy}^s \frac{\partial^2 w}{\partial x \partial y}$$

$$= \frac{\partial N_x}{\partial x}\frac{\partial w}{\partial x} + N_x\frac{\partial^2 w}{\partial x^2} + \frac{\partial N_y}{\partial y}\frac{\partial w}{\partial y} + N_y\frac{\partial^2 w}{\partial y^2} + \frac{\partial N_{xy}}{\partial x}\frac{\partial w}{\partial y} + \frac{\partial N_{xy}}{\partial y}\frac{\partial w}{\partial x} + 2N_{xy}\frac{\partial^2 w}{\partial x \partial y} \tag{6}$$

$$\delta w_s : \frac{\partial^2 M_x^s}{\partial x^2} + 2\frac{\partial^2 M_{xy}^s}{\partial x \partial y} + \frac{\partial^2 M_y^s}{\partial y^2} + \frac{\partial Q_{xz}}{\partial x} + \frac{\partial Q_{yz}}{\partial y} + N_x^s \frac{\partial^2 w}{\partial x^2} + N_y^s \frac{\partial^2 w}{\partial y^2} + 2N_{xy}^s \frac{\partial^2 w}{\partial x \partial y}$$

$$= \frac{\partial N_x}{\partial x}\frac{\partial w}{\partial x} + N_x\frac{\partial^2 w}{\partial x^2} + \frac{\partial N_y}{\partial y}\frac{\partial w}{\partial y} + N_y\frac{\partial^2 w}{\partial y^2} + \frac{\partial N_{xy}}{\partial x}\frac{\partial w}{\partial y} + \frac{\partial N_{xy}}{\partial y}\frac{\partial w}{\partial x} + 2N_{xy}\frac{\partial^2 w}{\partial x \partial y}$$

3 Solution Procedure for Mechanical Properties

The composite skins are cross-ply symmetrical laminated plates. There are no tension-bending coupling, tension-shear coupling and bending-torsion coupling. The composite skin needs low in-plane shear stiffness to achieve high in-plane strain capacity, so it is necessary to analyze the shear-driving force of composite skin. With reference to Fig. 3, the composite skin bears the shear-driving force (P_N) caused by shear-deformed parallelogram framework.

According to the deformation of the composite skin with the parallelogram frame, the strain of skin cells can be expressed as:

$$\varepsilon_{N_0 x} = 1 - \cos \beta, \ \varepsilon_{N_0 y} = 1 - \cos \alpha, \ \gamma_{N_0 xy} = \sin(\alpha + \beta) \tag{7}$$

where α and β are the shear-angle of wide side and long side; α_c and β_c are the critical shear angle of wide side and long side; $\varepsilon_{N_0 x}$, $\varepsilon_{N_0 y}$, and $\varepsilon_{N_0 xy}$ are the strain components associated with shear angle.

$$\theta = \alpha + \beta, \ \alpha = \arctan\left(\frac{L_x}{L_y}\right) - \arcsin\left(\frac{L_x}{L_y}\cos\left(\arctan\left(\frac{L_x}{L_y}\right) + \beta\right)\right) \tag{8}$$

where θ is the shear-angle of skin cells; θ_c is the critical shear angle of skin cells. By substituting the strain of skin cells into the constitutive relations of skin cells [22], the equations of in-plane force can be expressed as:
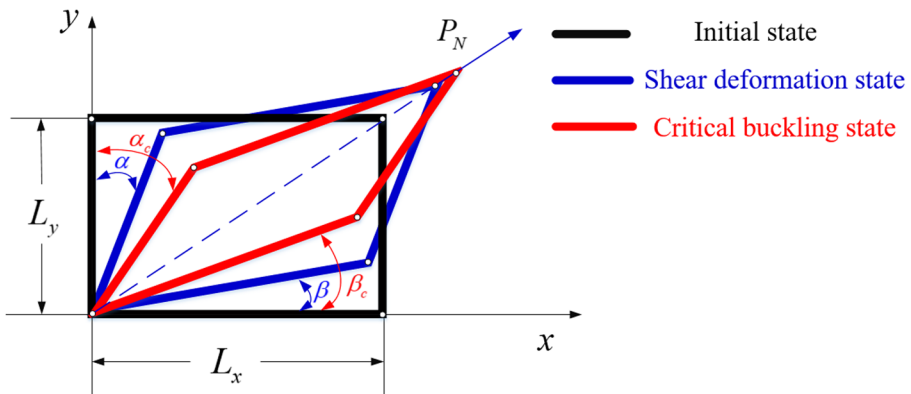

Fig. 3 The shear-deformation of skin cells

$$N_x^0 = A_{11}(1 - \cos \beta) + A_{12}(1 - \cos \alpha), N_y^0 = A_{12}(1 - \cos \beta) + A_{22}(1 - \cos \alpha), N_{xy}^0 = A_{66} \sin (\alpha + \beta)$$
(9)

where A_{11}, A_{12}, A_{22} and A_{66} are the plate stiffness coefficients, which are defined in [22]. Based on the principle of virtual work, the energy balance equation of composite skins can be expressed as:

$$W_1 - W_2 = 0$$
(10)

where W_1 is the strain energy; W_2 is the work done by the outside force. The strain energy and the work done by the outside force are expressed as:

$$W_1 = \sum_{k=1}^3 \int_{t_k}^{t_{k+1}} \int_0^{L_x} \int_0^{L_y} \left(\int \sigma_x^0 d\varepsilon_{N_0 x} + \int \sigma_y^0 d\varepsilon_{N_0 y} + \int \tau_{xy}^0 d\gamma_{N_0 xy} \right) dxdydz, \quad W_2 = \int_0^{\Delta L_d} P_N ds$$
(11)

where P_N is the in-plane shear driving force of composite skins, ΔL_d is the diagonal length variation of composite skins.

$$\Delta L_d = \sqrt{\left(L_x + L_y \sin(\alpha + \beta)\right)^2 + \left(L_y \cos(\alpha + \beta)\right)^2} - \sqrt{\left(L_x\right)^2 + \left(L_y\right)^2}$$
(12)

Substituting Eqs. (11) and (12) into Eq. (10), the shear-driving force can be obtained. The shear-driving force is related to the shear angle, length, width, and structural stiffness of the composite skin. According to the constraints of lines to the skin cell, the boundary is equivalent to the four sides simply supported. Following the Navier solution procedure, the displacement functions are expanded in the double triangular series [22, 23] to satisfy the simply supported boundary conditions of skins. By substituting the displacement functions into Eq. (6), the critical shear angle can be obtained. For this paper, although all the eigenvalues can be computed using the above method for each deformation mode of m (m is the half-wave number along the x-direction in the the double triangular series [22]) and n (n is the half-wave number along the y-direction in the the double triangular series [22]), the dominant eigenvalues corresponding to the minimum critical shear angle are of particular concern.

4 Experimental Measurements and Analysis

In order to verify the accuracy of theoretical analysis of shear driving force and critical shear angle of composite skins, the external mechanical properties of composite skin are tested and verified in this section. The Kevlar/carbon fiber hybrid composite skin sample used in this experiment is prepared by a separated fixture as shown in Fig. 4.

According to the preparation method of aramid fiber-reinforced epoxy nanocomposites [24], the preparation method of glass-fiber-reinforced epoxy nanocomposites [25] and the vacuum-assisted resin transfer molding method [26], the Kevlar/carbon fiber hybrid composite skin is manufactured as follows: (1) Evenly place the tensioned Kevlar ropes in the fixture; (2) Pour the liquid silicone rubber into the fixture and ensure that the Kevlar ropes are fully immersed; (3) Cover the pressing plate and wait for the rubber to cure; (4) Evenly place the carbon fiber rods orthogonal to the Kevlar ropes in the fixture; (5) Pour the liquid silicone rubber into the fixture and ensure that the carbon fiber rods are fully immersed; (6) Cover the pressing plate and wait for the rubber to cure; (7) Repeat steps (1)-(3) to complete the laying of the upper Kevlar ropes; (8) Complete the
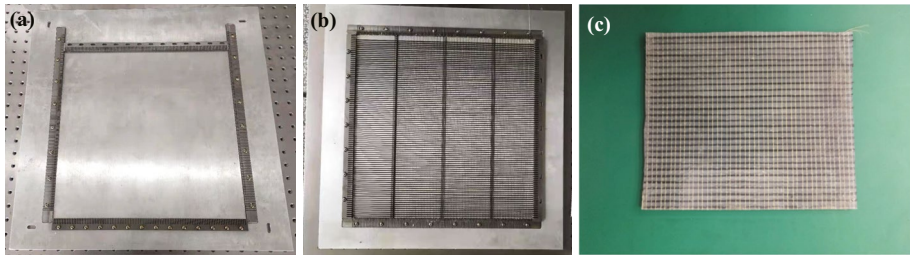
Fig. 4 Preparation of a Kevlar/carbon fiber hybrid composite skin. **a** a separated fixture, **b** the fixture covered with carbon fiber and Kevlar fiber, **c** the composite skin sample

preparation of composite skin sample. It is worth noting that the fiber spacing is uneven and there is initial deflection, which will affect the shear-driving force and critical shear angle. The mechanical properties of carbon fiber rod, Kevlar rope and silicone rubber matrix in the composite skin sample are shown in Table 1.

4.1 Verification and Analysis of Shear-driving Force

The shear-driving force test device was established as shown in Fig. 5. Black dye was added to the silicone rubber for subsequent experimental measurement. A rigid parallelogram frame ($d_1 = 0.12$ mm, $d_2 = 1.0$ mm, $L_x = 310$ mm, $L_x = 230$ mm) was used to simulate the framework cell, and the four sides of composite skins were stitched onto the framework to demonstrate the force state of the skin cells. Install the frame chuck on the diagonal rotating shaft of the parallelogram frame, and adjust the jaw of the electron tensile testing machine to lock the frame clamp. Through the change of the distance between the jaws of the electronic tensile testing machine, the composite skin is sheared, and the distance and the tensile force curve are measured at the same time.

As shown in Fig. 6, the test results of shear-driving force are in good agreement with the theoretical prediction results. It is proved that the combination of homogenization technique and the shear deformation plate theory is effective for Kevlar/carbon fiber hybrid composite skin structure. However, the theoretical solutions slightly underestimate the shear-driving force compared with the experimental results, since the arrangement of carbon fiber rods and Kevlar ropes is not completely uniform in the actual state, the contact effects between fiber and matrix and the driving force required for frame shear are not considered in the theoretical model. Typically, the theoretical prediction results are smaller than the experimental results when the shear angle is small, since the driving force required for frame deformation is not included in the theoretical calculation.

Table 1 Mechanical properties of base materials in the skin sample

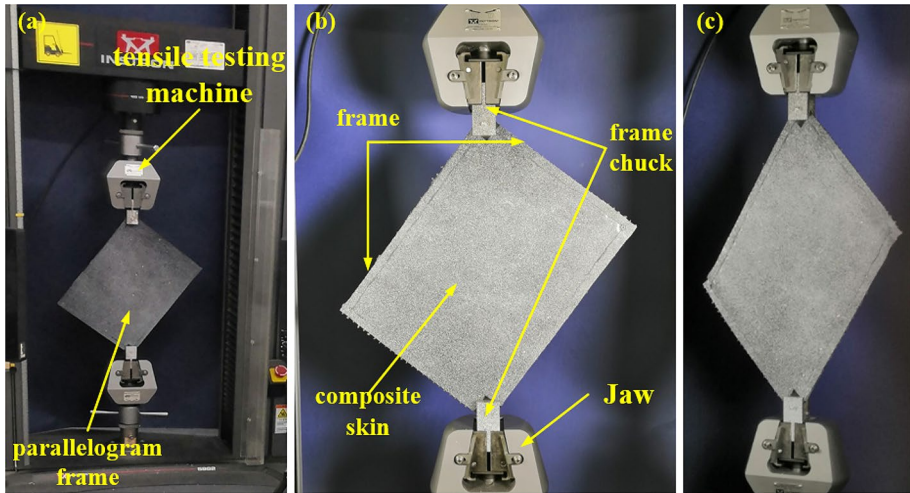| Mechanical properties	Silicone rubber	Kevlar fiber	Carbon fiber
Elastic modulus (Pa)	1.16×10^6	3.956×10^{10}	9.667×10^{10}
Poisson ratio	0.495	0.307	0.307
Shear modulus (Pa)	3.9×10^5	1.513×10^{10}	3.698×10^{10}

Fig. 5 Device for testing the shear driving force of composite skins: **a** the tensile testing machine, **b** the parallelogram frame with stitched a composite skin, and **c** the critical buckling state of composite skins

4.2 Verification and Analysis of Critical Shear Angle

In order to measure the critical shear angle of the composite skin during shear deformation, a critical shear angle measuring device was designed. As shown in Fig. 7, the diagonal structures of the parallelogram frame stitched with the composite skin are connected with the electron tensile testing machine. Through the movement of the electron tensile testing machine, the diagonal length of the parallelogram frame is changed to realize the shear deformation of the composite skin. In order to measure the smoothness of skin surface, digital image correlation technology (DIC) is used as shown in Fig. 7. Due to the light transmission of the rubber matrix, the image acquisition effect is poor. In order to get more accurate measurement results, black dye was added into silicone rubber for subsequent experimental measurement.

Fig. 6 Comparison of the shear-driving force of morphing skin samples
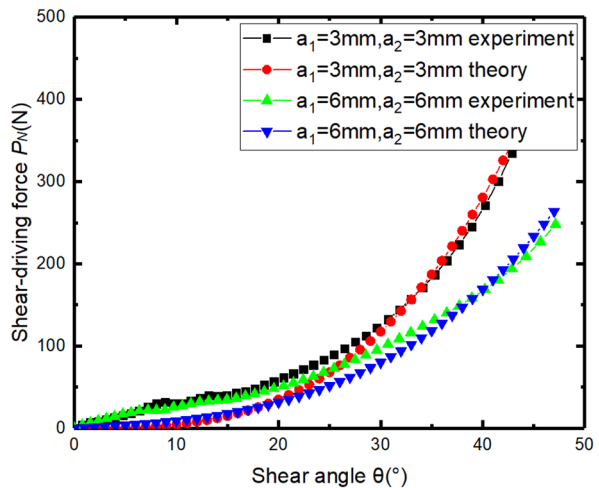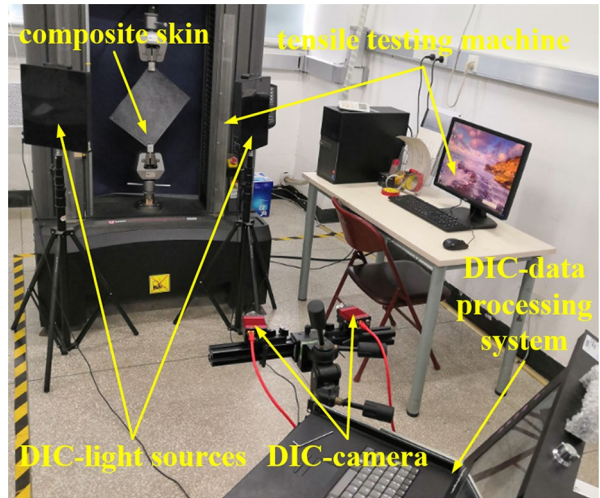
Fig. 7 Device for testing the critical shear angle of composite skins

The curvature diagrams of three morphing skin samples ($d_1 = 0.12$ mm, $d_2 = 1.5$ mm) during the shear deformation process are shown in Fig. 8. The curvature of composite skins is close to zero in the initial state. As the shear angle increases, the fibers shear the rubber matrix and makes it extruded. Because the elastic modulus of fiber is much larger than that of rubber matrix, the deformation is mainly caused by rubber matrix. Moreover, due to the

(a) $a_1 = 4$mm, $a_2 = 4$mm $\qquad$ **(b)** $a_1 = 8$mm, $a_2 = 8$mm $\qquad$ **(c)** $a_1 = 12$mm, $a_2 = 12$mm
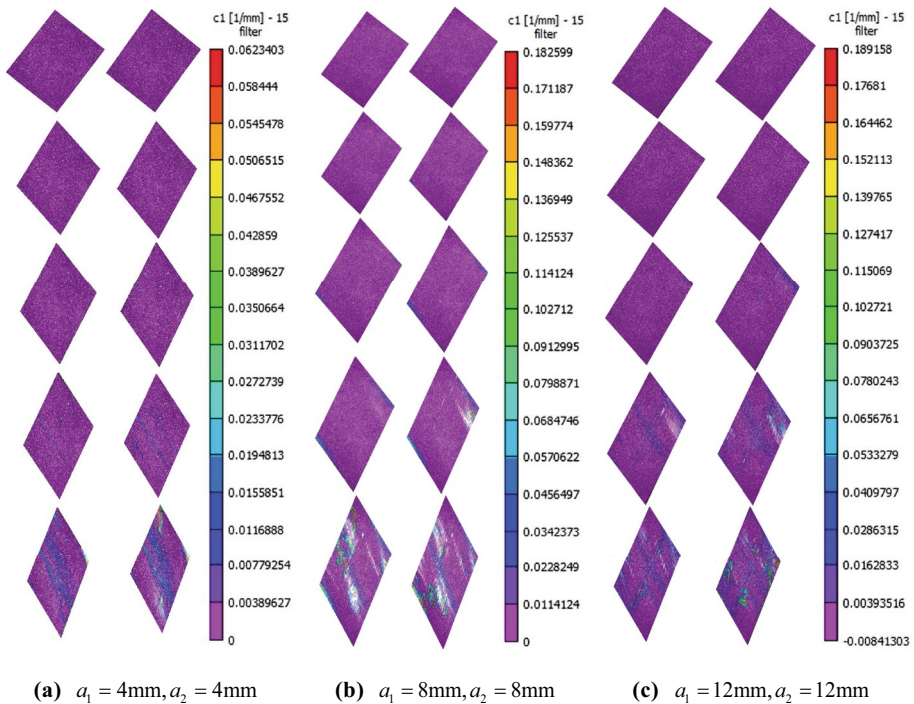
Fig. 8 Comparison of critical shear angle of three morphing skin samples

Table 2 Comparison of theoretical and experimental values of critical shear angle

Skin parameters	Experimental results	Theoretical results
$a_1 = 4$ mm, $a_2 = 4$ mm	32.33°	34.88°
$a_1 = 8$ mm, $a_2 = 8$ mm	23.04°	27.38°
$a_1 = 12$ mm, $a_2 = 12$ mm	18.27°	21.63°

tight arrangement of fibers, the curvature increases but the change is small. As the shear angle continued to increase, the positive compressive stress of the rubber matrix increased, and the reverse flexural force of the fibers increased. When the shear angle increases to the critical shear angle, the fibers are deflected under the deformation and compression of the rubber matrix. At the same time, the curvature of the composite skin sample changes suddenly, resulting in the skin wrinkling.

The experimental results of critical shear angle of three skin samples are extracted from Fig. 8. As is shown in Table 2, good agreement between experimental results and theoretical predictions using CPT model is achieved. The effectiveness of the refined shear deformation plate theory is thus demonstrated for Kevlar/carbon fiber hybrid composite skins. However, the theoretical solutions of the critical shear angle are deviated from the experimental results, since the contact effect between the fiber reinforcement and the matrix is not considered in the theoretical model.

5 Parametric Study of Mechanical Properties

5.1 Effects of Carbon Fiber Diameter and Kevlar Diameter

As can be observed from Fig. 9, the shear-driving force the composite skins ($a_1 = 6$ mm, $a_2 = 6$ mm) increase with increasing Kevlar diameter d_1 and carbon fibers diameter d_2. Moreover, it is apparent from Fig. 9 that carbon fiber diameter d_2 is more pronounced for the shear-driving force compared with Kevlar diameter d_1. This implies that the shear-driving force of the composite skins is mainly affected by carbon fiber due to the higher Young's Modulus of carbon fiber material.
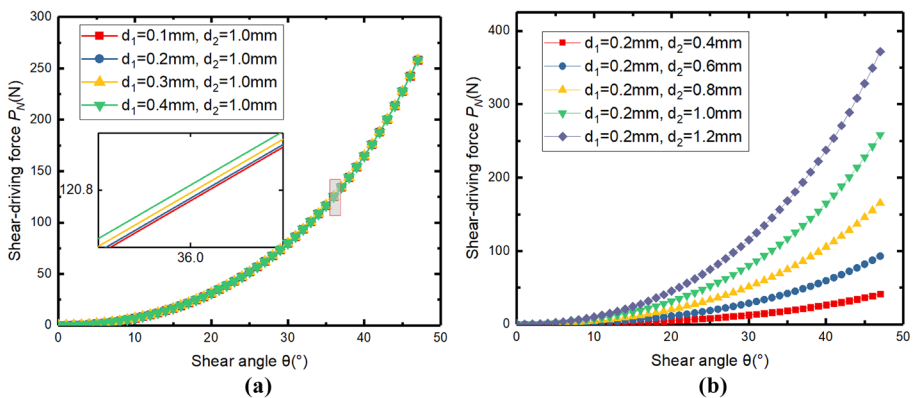

Fig. 9 Effects of the carbon fiber diameter and Kevlar diameter on shear-driving force: **a** Kevlar diameter; **b** carbon fiber diameter
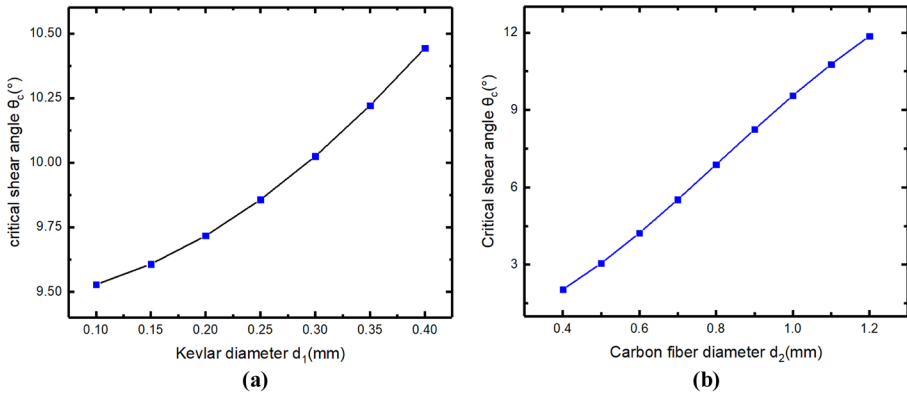
Fig. 10 Effects of the carbon fiber diameter and Kevlar diameter on critical shear angle: **a** Kevlar diameter; **b** carbon fiber diameter

To explore the influence of Kevlar diameter d_1 and carbon fibers diameter d_2, Fig. 10 plots the critical shear angle of the composite skins ($a_1 = 6$ mm, $a_2 = 6$ mm) with different fiber diameter and Kevlar diameter. It is striking to find that the increase of fiber diameter and Kevlar diameter increases the critical shear angle of composite skins. However, increasing the carbon fiber diameter has a greater impact on the critical shear angle of the composite skin than increasing the Kevlar diameter.

5.2 Effects of Carbon Fiber Spacing and Kevlar Spacing

Effects of the Kevlar spacing a_1 and carbon fiber spacing a_2 upon the shear-driving force of the composite skins ($d_1 = 0.12$ mm, $d_2 = 1.0$ mm) is presented in Fig. 11. It is seen from Fig. 11 that the shear-driving force decreases monotonically with increasing Kevlar spacing a_1 and carbon fiber spacing a_2, because the in-plane stiffness of the composite skins decreases rapidly as soon as the volume fraction of fiber decreases. Moreover, carbon fiber spacing a_2 is more pronounced for the shear-driving force compared with
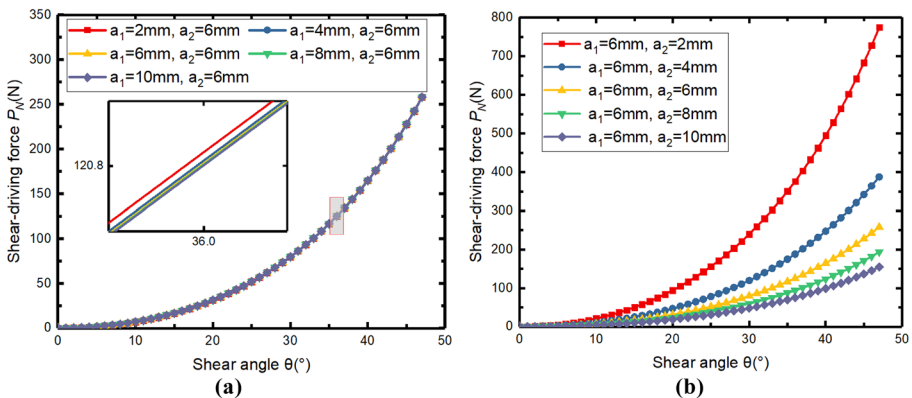

Fig. 11 Effects of the carbon fiber spacing and Kevlar spacing on shear-driving force with: **a** Kevlar spacing; **b** carbon fiber spacing
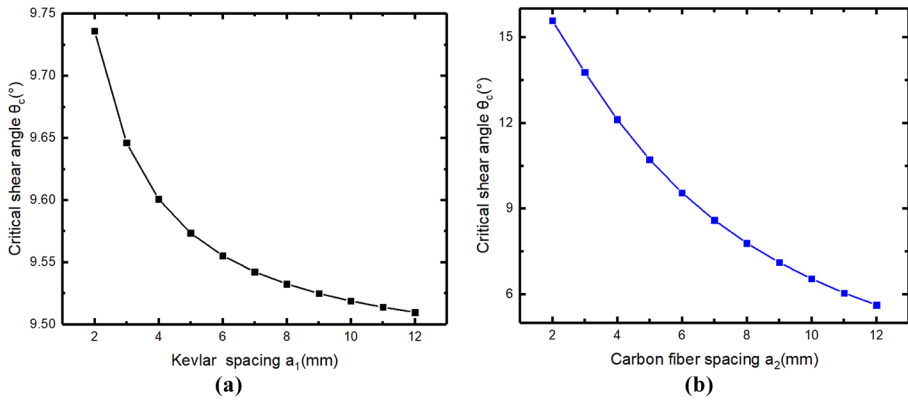
Fig. 12 Effects of the carbon fiber spacing and Kevlar spacing on critical shear angle **a** Kevlar spacing; **b** carbon fiber spacing

Kevlar spacing a_1. This implies that the shear-driving force is mainly affected by carbon fiber.

To explore the influence of the Kevlar spacing a_1 and carbon fiber spacing a_2, Fig. 12 plots the critical shear angle of the composite skins ($d_1 = 0.12$ mm, $d_2 = 1.0$ mm) with different the Kevlar spacing and carbon fiber spacing. It is striking to find that the increase of Kevlar spacing and carbon fiber spacing decreases monotonically the critical shear angle of composite skins, since the buckling load of the composite skins decreases as soon as the volume fraction of fiber decreases. Therefore, decreasing carbon fiber spacing has more influence on the critical shear angle of composite skins than decreasing Kevlar spacing.

5.3 Effect of Skin Thickness

Influence of skin cell thickness t upon the shear-driving force and critical shear angle that plotted as a function of shear-angle change and skin cell thickness change for the composite skins ($d_1 = 0.12$ mm, $d_2 = 1.0$ mm, $a_1 = 6$ mm, $a_2 = 6$ mm) is presented in Fig. 13. It is striking to find that the increase of thickness slightly increases the shear-driving force
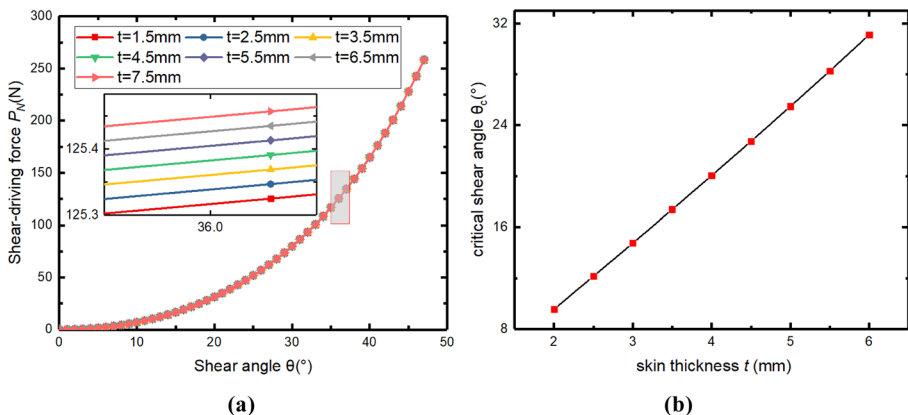

Fig. 13 Effect of the composite skin thickness t on **a** shear-driving force and **b** critical shear angle
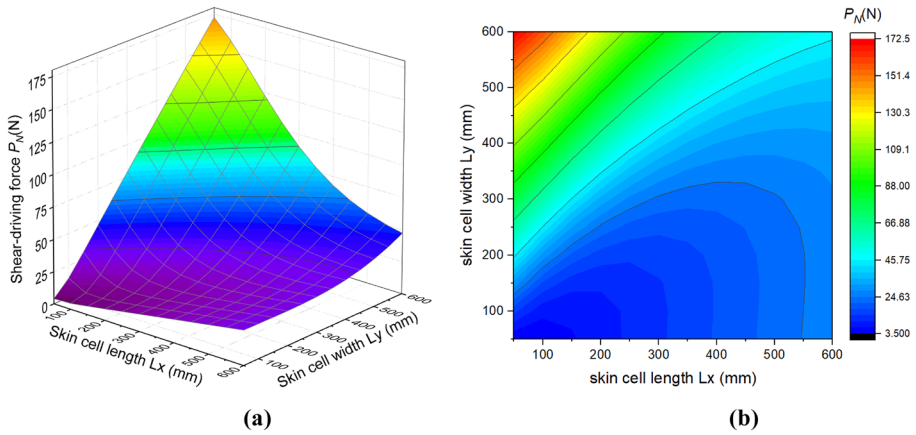
Fig. 14 Effect of the composite skin length L_x and width L_y on shear-driving force: **a** 3D three-dimensional view and **b** two-dimensional contour view

of composite skins. This phenomenon is due mainly to the driving force required for the deformation of the reinforcing fiber being much greater than the driving force required. However, the critical shear angle of composite skin increases significantly with the increase of thickness. Therefore, increasing the thickness of composite skins can effectively increase the critical shear angle while keeping other parameters of the composite skin unchanged.

5.4 Effect of Skin Cell Length and Width

Figure 14 shows the effects of the skin cell length L_x and width L_y upon the shear-driving force of composite skins for $a_1 = 6$ mm, $a_2 = 6$ mm, $d_1 = 0.12$ mm, $d_2 = 1.0$ mm, $\theta = 20°$. When the L_x or L_y is relatively small, the shear-driving force increases rapidly with increasing L_x and L_y. When the L_x or L_y is large, the shear driving force first decreases and
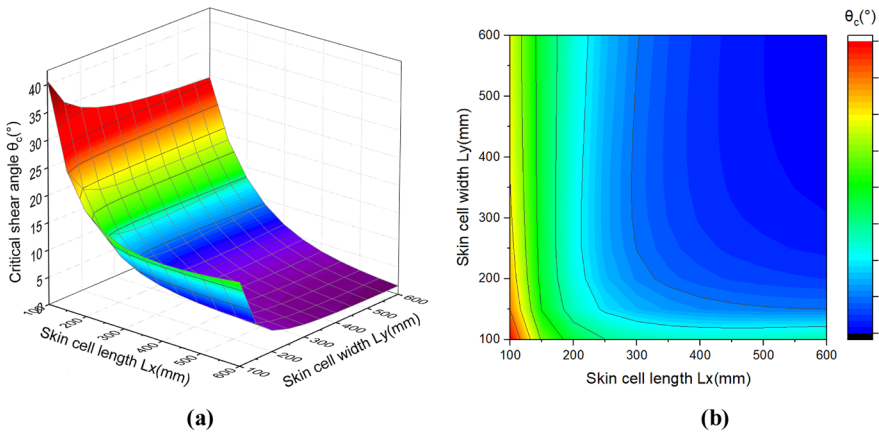

Fig. 15 Effect of the composite skin length L_x and width L_y on critical shear angle: **a** 3D three-dimensional view and **b** two-dimensional contour view
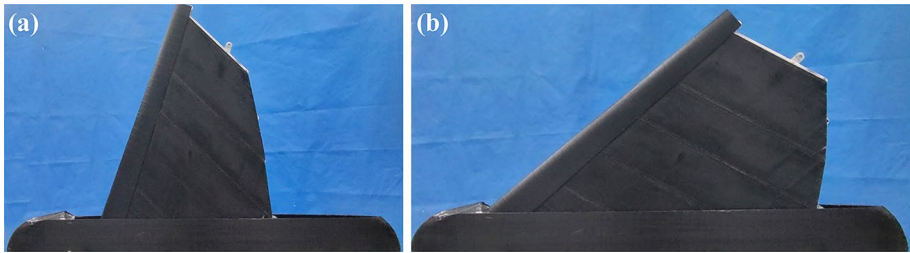
Fig. 16 Morphing process of variable-sweep wing during ground test: **a** small sweep angle state; **b** large sweep angle state

then increases with increasing L_x and L_y. Moreover, the composite skin width L_y is more pronounced for the shear-driving force compared with the length L_x. This implies that the appropriate length L_x and width L_y can effectively reduce the shear-driving force of the skin.

The effect of the length L_x and width L_y on the critical shear angle of the composite skins ($a_1 = 6$ mm, $a_2 = 6$ mm, $d_1 = 0.12$ mm, $d_2 = 1.0$ mm) is evaluated and shown in Fig. 15. With the increase of the composite skin length and width, the critical shear angle decreases. Moreover, it can be seen that the rate of change on the critical shear angle becomes smaller with the increase of the composite skin length and width. This implies reducing the length and width of skin cells can increase the range of smooth deformation.

6 Utilization of Skin on Demonstrator Wing

A variable-sweep wing in which the Kevlar/carbon fiber hybrid composite skin is utilized has been manufactured and tested on ground. The morphing wing is composed of morphing skeleton and multiple morphing composite skins. The wing skeleton consists of several parallelogram morphing frames. The composite skins will be fixed on the upper and lower surfaces of the parallelogram morphing frames by mechanical connection to form a smooth and continuous surface. In order to make the variable-sweep wing smooth and continuous within the range of 20°-60° sweep angle, the composite skin parameters are set to $a_1 = 4$ mm, $a_2 = 4$ mm, $d_1 = 0.12$ mm, $d_2 = 1.5$ mm, $t = 4$ mm based on the above analysis. The bending stiffness and torsion stiffness of the morphing wing are mainly provided by the morphing skeleton. The composite skin not only can realize large-scale continuous deformation, but also has certain bearing capacity which can keep the wing surface smooth and continuous under the aerodynamic force. The sweep angle is changed by changing the length of the parallelogram diagonal, and the motors are utilized as morphing actuators. The manufacturing and the morphing test on ground are shown in Fig. 16.

7 Conclusions

In this study, the Kevlar/carbon fiber hybrid composite skin that can be smoothly and continuously sheared is proposed and applied. Moreover, the shear driving force and critical shear angle of the hybrid composite skin are theoretically investigated. Based on the principle of virtual work and the classical plate theory, the mathematical model is developed

for the shear-driving force and critical shear angle of the Kevlar/carbon fiber hybrid composite skins. The theoretical and experimental results of the shear driving force and the critical shear angle are in good agreement, which verifies the accuracy of the theoretical model. Aspects including the carbon fiber diameter, carbon fiber spacing, together with the length and width of skin cell affect significantly the shear-driving force of Kevlar/carbon fiber hybrid composite skins, but the influences of Kevlar diameter, Kevlar spacing and thickness are relatively non-significant. Aspects including the carbon fiber diameter, carbon fiber spacing, Kevlar diameter, Kevlar spacing, thickness, together with the length and width of skin cell affect significantly the critical shear angle of Kevlar/carbon fiber hybrid composite skins. Based on the above analysis, the Kevlar/carbon fiber hybrid composite skin($a_1 = 4$ mm, $a_2 = 4$ mm, $d_1 = 0.12$ mm, $d_2 = 1.5$ mm, $t = 4$ mm, $L_x = 310$ mm, $L_y = 230$ mm) was applied to achieve smooth and continuous deformation of a shear variable-sweep wing in the range of 20°-60° sweep angle.

Data Availability The datasets used and analysed during the current study are available from the corresponding author on reasonable request. The authors declare that there is no conflict of interests regarding the publication of this article.

References

1. Barbarino, S., Bilgen, O., et al.: A Review of Morphing Aircraft. J. Intell. Mater. Syst. Struct. **22**(9), 823–877 (2011)
2. Seigler, T.M., Neal, D.A., et al.: Modeling and Flight Control of Large-Scale Morphing Aircraft. J. Aircraft. **44**(4), 1077–1087 (2007)
3. Anderse, G. R., Cowan, D. L., et al.: Aeroelastic Modeling, Analysis and Testing of a Morphing Wing Structure. In: 48rd AIAA/ASME/ASCE/AHS/ASC Structures, Structural Dynamics, and Materials Conference. Honolulu, Hawaii (2007)
4. Bowman, J., Sanders, B., et al.: Development of Next Generation Morphing Aircraft Structures. In: 48rd AIAA/ASME/ASCE/AHS/ASC Structures, Structural Dynamics, and Materials Conference. Honolulu, Hawaii (2007)
5. Thill, C., Etches, J.A., et al.: Morphing skins. Aeronaut. J. **112**(1129), 117–139 (2008)
6. Grant, D.T., Abdulrahim, M., Lind, R.: Flight dynamics of a morphing aircraft utilizing independent multiple-joint wing sweep. Int. J. Micro. Air. Veh. **2**(2), 91–106 (2010)
7. Keihl, M.M., Bortolin, R.S., et al.: Mechanical properties of shape memory polymers for morphing aircraft applications. Proc. SPIE. Int. Soc. Opt. Eng. **5762**, 143–151 (2005)
8. Olympio, K.R., Asheghian, L., Gandhi, F., et al.: Design of a Flexible Skin for a Shear Morphing Wing. J. Intell. Mater. Syst. Struct. **21**(17), 1755–1770 (2010)
9. Laila, A., Greg, R., Andrew, E., et al.: Shear Morphing Skins-Simulation and Testing of Optimized Design. J. Intell. Mater. Syst. Struct. **22**(9), 945–959 (2011)
10. Phan, N.D., Reddy, J.N.: Analyses of Laminated Composite Plates using a Higher-order Deformation Theory. Int. J. Num. Meth. Eng. **21**(12), 2201–2219 (1985)
11. Karama, M., Afaq, K.S., Mistou, S.: Mechanical behavior of laminated composite beam by new multilayered laminated composite structures model with transverse shear stress continuity. Int. J. Solids. Struct. **40**(6), 1525–1546 (2003)
12. Mantari, J.L., Oktem, A.S., Soares, C.G.: A new trigonometric shear deformation theory for isotropic, laminated composite and sandwich plates. Int. J. Solids. Struct. **49**(1), 43–53 (2012)
13. Ghugal, Y.M., Pawar, M.D.: Buckling and vibration of plates by hyperbolic shear deformation theory. J. Aerosp. Eng. Technol. **1**(1), 1–12 (2011)

14. Belabed, Z., et al.: An efficient and simple higher order shear and normal deformation theory for functionally graded material (FGM) plates. Compos. B. Eng. **60**, 274–283 (2014)
15. Grover, N., Singh, B.N., Maiti, D.K.: Analytical and finite element modeling of laminated composite and sandwich plates: an assessment of a new shear deformation theory for free vibration response. Int. J. Mech. Sci. **67**, 89–99 (2013)
16. Sabri, F., Meguid, S.A.: Wrinkling prediction of laminated composite panels under in-plane shear deformation. Acta. Mech. **232**, 57–72 (2021)
17. Ni, Q.Q., Xie, J., Iwamoto, M.: Buckling analysis of laminated composite plates with arbitrary edge supports. Compos. Struct. **69**, 209–217 (2005)
18. Dash, P., Singh, B.N.: Buckling and post-buckling of laminated composite plates. Mech. Res. Commun. **46**, 1–7 (2012)
19. Thai, H.T., Vo, T.P.: A new sinusoidal shear deformation theory for bending, buckling, and vibration of functionally graded plates. Appl. Math. Model. **37**(5), 3269–3281 (2013)
20. Thakur, B.R., Verma, S., et al.: Geometrically nonlinear dynamic analysis of laminated composite plate using a nonpolynomial shear deformation theory. Int. J. Nonlin. Mech. **128**(103635), 1–19 (2021)
21. Aydogdu, M.: Comparison of various shear deformation theories for bending, buckling, and vibration of rectangular symmetric cross-ply plate with simply supported edges. J. Compos. Mater. **40**(23), 2143–2155 (2006)
22. Yang, G., Guo, H., Xiao, H., et al.: Out-of-Plane Stiffness Analysis of Kevlar/Carbon Fiber Hybrid Composite Skins for a Shear Variable-Sweep Wing. Appl. Compos. Mater. **28**, 1653–1673 (2021)
23. Shen, G.: Mechanics of Composite Materials, 2nd edn. Tsinghua University Press, Beijing (2006)
24. Demircan, G., Kisa, M., Ozen, M., et al.: Surface-modified alumina nanoparticles-filled aramid fiber-reinforced epoxy nanocomposites: preparation and mechanical properties. Iran. Polym. J. **29**, 253–264 (2020)
25. Demircan, G., Kisa, M., Ozen, M., et al.: Quasi-Static Penetration Behavior of Glass-Fiber-Reinforced Epoxy Nanocomposites. Mech. Compos. Mater. **57**, 503–516 (2021)
26. Ozen, M., Demircan, G., Kisa, M., Ilik, Z.: Investigation of usability of waste textile fabrics in composites. Emerg. Mater. Res. **9**(1), 18–23 (2020)

Publisher's Note Springer Nature remains neutral with regard to jurisdictional claims in published maps and institutional affiliations.